Heterogeneous Integration of Thin-Film Organic and Inorganic Devices for Optical Based Bioelectrical and Chemical Sensing

He Ding, Yanxiu Peng, Guoqing Lv, Yang Xie, Junyu Chen, Zhao Shi, Yuping Deng, Lan Yin, Jian Yang, Yongtian Wang, and Xing Sheng

(Invited Paper)

***Abstract*—Directly visualizing electrical and chemical signals via optical approaches is an effective and powerful method for analyzing biological activities in a remote and high-throughput manner. Here we develop a heterogeneously integrated optoelectronic sensor that optically monitors the changes of bioelectrical and biochemical signals. Fabricated via epitaxial liftoff and transfer printing, the thin-film, microscale sensor combines a photodiode and a light-emitting diode (LED) made of inorganic III–V compound semiconductor heterostructures, as well as an organic electrochemical transistor (OECT). Ascribed to the matching condition among the heterogeneously integrated components, luminescent emissions of the sensor, which can be captured with a fluorescence microscope, dynamically respond to input electrical signals and are systematically characterized. Through voltage dependent luminance variations, the device optically records synthesized electrocardiography (ECG) signals with peak amplitudes from 100 mV to 10 mV. Furthermore, the integrated sensor is capable of selectively detecting calcium variations when immersing into the aqueous solution. The integrated sensor combines the advantages of inorganic and organic semiconductors and offers opportunities to wirelessly detect biological activities at a large scale.**

***Index Terms*—Biological sensors, heterogeneous integration, optoelectronics, transfer printing.**

Manuscript received 23 August 2022; revised 21 October 2022; accepted 22 October 2022. Date of publication 25 October 2022; date of current version 9 November 2022. This work was supported in part by the National Natural Science Foundation of China under Grants 62005016, 61874064, and 52272277, in part by Beijing Municipal Natural Science Foundation under Grant 4202032, in part by EnSan Frontier Innovation Foundation under Grant 2022003, and in part by Tsinghua University Initiative Scientific Research Program. *(Corresponding authors: He Ding; Xing Sheng.)*

He Ding, Yanxiu Peng, Guoqing Lv, Jian Yang, and Yongtian Wang are with the Beijing Engineering Research Center of Mixed Reality and Advanced Display, School of Optics and Photonics, Beijing Institute of Technology, Beijing 100081, China (e-mail: heding@bit.edu.cn; yanxiup@foxmail.com; 1026678201@qq.com; jyang@bit.edu.cn; wyt@bit.edu.cn).

Yang Xie, Junyu Chen, Zhao Shi, and Xing Sheng are with the Department of Electronic Engineering, Beijing National Research Center for Information Science and Technology, Institute for Precision Medicine, Center for Flexible Electronics Technology, and IDG/McGovern Institute for Brain Research, Tsinghua University, Beijing 100084, China (e-mail: yangxie2019@163.com; cjy22@mails.tsinghua.edu.cn; shizhaohust@163.com; xingsheng@tsinghua.edu.cn).

Yuping Deng and Lan Yin are with the School of Materials Science and Engineering, Tsinghua University, Beijing 100084, China (e-mail: dengyp18@mails.tsinghua.edu.cn; lanyin@tsinghua.edu.cn).

Color versions of one or more figures in this article are available at https://doi.org/10.1109/JSTQE.2022.3217070.

Digital Object Identifier 10.1109/JSTQE.2022.3217070

I. Introduction

RECORDING electrical and chemical signals of biological cells, tissues, organs and systems are of great interest in understanding biological activities and are critically relevant to the development of biomedical devices like prostheses, brain-machine interfaces, and pacemakers [1], [2], [3], [4], [5], [6], [7], [8]. Currently, representative biological sensing methods are based on tools acquiring electrical and/or optical signals, and each approach exhibits its own advantages and challenges in aspects of invasiveness, sensitivity, selectivity, dynamics, throughput, etc [1], [2], [3], [4], [5], [9], [10]. The standard patch-clamp technique can record intracellular and extracellular electrophysiological activities with high signal-to-noise ratios and temporal resolutions, but its recording capacity is limited to a few channels [11]. Recently developed microelectrode arrays and transistors enable multiplexed recording sites with small footprints and high sensitivities, but they still associate with complex and tethered readout circuits design [2], [3], [6], [10]. On the other hand, genetically encoded optical indicators can selectively respond to variations of voltage, ions and neurotransmitters reflected by their fluorescence fluctuations, but genetic modifications via viral injection hinder their immediate use in medical fields [12], [13]. [14], [15]. In addition, certain organic based fluorescence proteins and dyes suffer from photostability and toxicity. Considering these challenges related to existing electronic and optical methods, there is still a pressing need to realize a sensing method to remotely visualize biological signals in real-time [9], [16].

The near-infrared (NIR) spectral range between 700 nm and 1000 nm, which functions as an optical window for biological applications, presents deep tissue penetration, low thermal effect, and non-interfering autofluorescence, and has been widely used for optical stimulating and recording in biomedicine [17], [18]. On the one hand, optoelectronic devices based on single crystalline, inorganic III–V compound semiconductors can accomplish optical detection and emission in the NIR range with high energy conversion efficiencies and operation stability. We have recently reported an upconversion device based on an III–V semiconductor heterostructure that can convert low-energy photons at a wavelength of ∼810 nm to high-energy photons at a

1077-260X © 2022 IEEE. Personal use is permitted, but republication/redistribution requires IEEE permission.
See https://www.ieee.org/publications/rights/index.html for more information.

Authorized licensed use limited to: Tsinghua University. Downloaded on November 12,2022 at 07:43:25 UTC from IEEE Xplore. Restrictions apply.

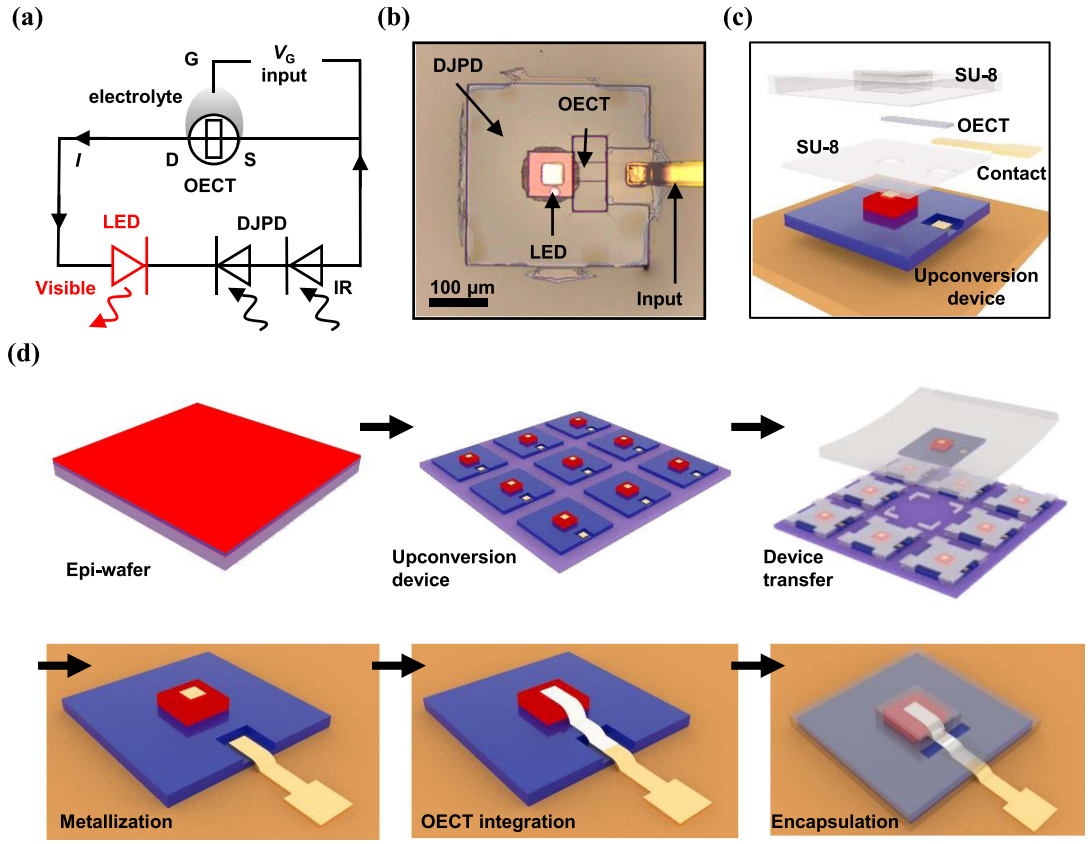

Fig. 1. Design and fabrication of the heterogeneously integrated, thin-film optoelectronic device for sensing. (a) Circuit diagram of the device design, including an InGaP-based red LED and a GaAs-based double junction photodiode (DJPD) to form an infrared-to-visible upconversion device, which are serially connected to a PEDOT:PSS based organic electrochemical transistor (OECT). G: gate; D: drain; S: source. (b) Optical image (top view) and (c) exploded schematic illustration of the integrated device, in which the OECT channel is exposed to the electrolyte and the external voltage signal is applied to the input electrode. (c) Schematic illustration of the process flow for fabricating the integrated sensor, with main steps including lithographic patterning, sacrificial layer removal, transfer printing, metallization, OECT integration, and encapsulation.

wavelength of ~625 nm, with a low excitation power, a high conversion efficiency and fast dynamics [19], [20]. In addition, the unique "photon-electron-photon" conversion mechanism of this optoelectronic device generates internal voltages and currents that can possibly interact with other sensing elements [21], [22]. On the other hand, organic based electronic materials (for example, poly(34-ethylenedioxythiophene) polystyrene sulfonate, or PEDOT:PSS) holds peculiar features when interfacing with biological systems, including low contact impedance, high ion sensitivity and desirable biocompatibility [7], [23], [24], [25], [26], [27], [28]. Therefore, we envision that the combination of inorganic and organic devices can leverage their individual capabilities of optical reception/emission and electronic/chemical sensing, and promises unprecedented applications in biological sensing.

In this study, we heterogeneously integrate inorganic and organic based thin-film microscale devices for optically sensing bioelectrical and chemical signals. Via transfer printing and lithographic patterning, infrared-to-visible optical upconversion devices made of III–V compounds and a PEDOT:PSS based OECT are vertically assembled on flexible substrates. Under infrared excitation, the integrated device generates fluorescence dynamically responding to input electrical signals, which can be remotely recorded by a microscope. Proof-of-concept demonstrations show that synthesized ECG signals and calcium ion concentrations can be optically detected. Such a device concept establishes the union of inorganic and organic semiconductors and enables an effective solution for optical monitoring of biological activities.

II. Results and Discussion

Our developed sensor is based on the heterogeneous integration of thin-film, microscale inorganic and organic semiconductoring devices, with main components including a gallium arsenide (GaAs) based double junction photodiode (DJPD) (with a lateral dimension of ~300 × 300 μm^2), an indium gallium phosphide (InGaP) based red LED (~90 × 90 μm^2), and a PEDOT:PSS based OECT (channel length ~55 μm, width ~30 μm, thickness ~100 nm). Fig. 1(a) presents the schematic circuit diagram of the integrated sensor. The combination of the GaAs DJPD and the InGaP LED forms an optoelectronic upconversion device, which can be excited by infrared illumination and generate red emission [19]. The source (S) and the drain (D) of the OECT are connected to anodes of the DJPD and the LED, respectively, with a silver/silver chloride

Authorized licensed use limited to: Tsinghua University. Downloaded on November 12,2022 at 07:43:25 UTC from IEEE Xplore. Restrictions apply.

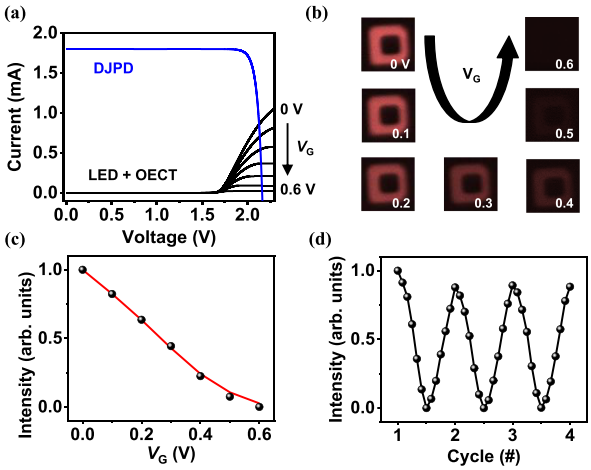

Fig. 2. Operating mechanism and performance of the heterogeneously integrated sensor. (a) Calculated current–voltage characteristics of the DJPD (red) under an excitation power density of ∼2 W cm^{-2} at a wavelength of ∼810 nm as well as combined red LED and OECT (black) under different input gate voltages (V_G) from 0 V to 0.6 V. (b) Microscopic images showing the red emission from the LED under V_G from 0 V to 0.6 V. (c) Calculated (red line) and measured (black dots) upconversion emission intensity as a function of V_G. (d) Cycled test of the emission intensity by applying V_G repeatedly from 0 V to 0.6 V.

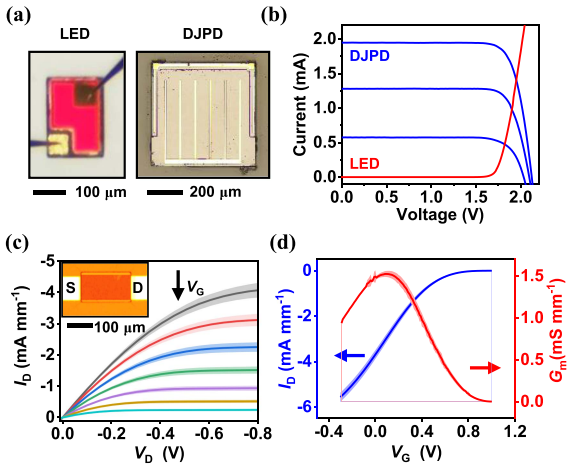

Fig. 3. Operating characteristics of individual components in the heterogeneously integrated sensor. (a) Microscope images of an InGaP red LED and a GaAs DJPD. (b) Measured current–voltage curves for the LED (red curve) and the DJPD (blue curve) under different illumination intensities (0.24, 0.52, and 0.80 W cm^{-2}, at 810 nm). (c) Microscope image of an OECT (inset) and its output (I_D–V_D) characteristics at various V_G (0, 0.1, 0.2, 0.3, 0.4, and 0.5, and 0.6 V) in the 10 mM NaCl solution over 5 hours. (d) Transfer (I_D–V_G) characteristics of the OECT and the corresponding transconductance (G_m) at $V_D = -0.6$ V.

(Ag/AgCl) wire as the gate electrode (G) in the 10 mM NaCl aqueous solution. Since the upconversion device and the OECT are connected in series, the channel current of the OECT can be modulated via the changes of external gate voltage (V_G) or the electrolyte concentration (presented as the grey shaded area in Fig. 1(a)). Fig. 1(b) shows the top-view microscope image of the heterogeneously integrated sensor (with a total thickness of ∼16 μm) transferred on a polyimide substrate, with the LED emitting red light under infrared excitation. Its corresponding schematic image (exploded view) is illustrated in Fig. 1(c). Fig. 1(d) details the device fabrication process. The III–V based upconversion device is formed by epitaxial growth and lithographic etching, followed by sacrificial layer removal and transfer printing on polyimide with polydimethylsiloxane (PDMS) stamps [19]. Spin-coated and patterned PEDOT:PSS forms the channel of the OECT. Finally, the device is encapsulated with SU-8 epoxy with only the PEDOT:PSS layer exposed to the electrolyte. With the input electrode connecting to the external Ag/AgCl wire, voltage signals can be applied to the electrode as V_G. Although our current device has a dimension of more than 100 μm, further miniturazation with advanced lithographic tools should be feasible to form device arrays with pixel sizes less than 10 μm.

The functional sensor is powered by an external excitation laser source at a center wavelength of ∼810 nm, which is absorbed by the GaAs DJPD and converted into electric power to drive the InGaP LED and the OECT. Detailed theoretical calculations are provided in the methods. Fig. 2(a) plots the calculated current–voltage curves of the DJPD under an excitation intensity of ∼2 W cm^{-2} as well as the serially connected LED and OECT with applied V_G from 0 V to 0.6 V in a step of 0.1 V. The intersection points of the two curves mark the working conditions of the integrated sensor at different V_G, indicating the injected currents for LED emission. The corresponding LED luminescence images are captured by a fluorescence microscope equipped with a complementary metal-oxide-semiconductor (CMOS) camera. As shown in Fig. 2(b), the red emission from the LED becomes dimmer with increased V_G. The measured results are in accordance with the calculations (Fig. 2(c), with a coefficient of determination of 0.99). Furthermore, the optical signals of the integrated sensor are fully reversible under cyclically applied V_G, owing to the fast doping and dedoping processes of the PEDOT:PSS based OECT structure. These results demonstrate the potential of optical based voltage sensing with such a heterogeneously integrated sensor.

To further grasp the sensing mechanism of the heterogeneously integrated device, we analyze the characteristics of device components with individually fabricated LED, DJPD, and OECT. Microscopic photographs in Fig. 3(a) illustrate an InGaP LED (left, 190 × 140 μm^2) and a GaAs DJPD (right, 700 × 700 μm^2), with the device epitaxial structures identical to those in the integrated sensor. Their current–voltage characteristics are measured and plotted in Fig. 3(b). The GaAs DJPD presents an open-circuit voltage close to 2 V, which is sufficient to turn on the InGaP LED. The inset of Fig. 3(c) shows a PEDOT:PSS OECT with a channel length of ∼200 μm and width of ∼100 μm immersed in a 10 mM NaCl solution, and the electrical characteristics are measured with a Ag/AgCl wire as the gate electrode. Due to the absence of gate oxide and the high conductivity of PEDOT:PSS, the OECT shows a low-operation voltage, which is suitable for working in aqueous environments. The output curves of OECT under different V_G immersed in 10 mM NaCl solution within 5 hours are shown in Fig. 3(c), and the coefficient of variation is ∼6% compared to the initial drain current at a maximum V_G of 0.1 V and V_D of −0.6 V. A PEDOT:PSS based OECT typically operates

Authorized licensed use limited to: Tsinghua University. Downloaded on November 12,2022 at 07:43:25 UTC from IEEE Xplore. Restrictions apply.

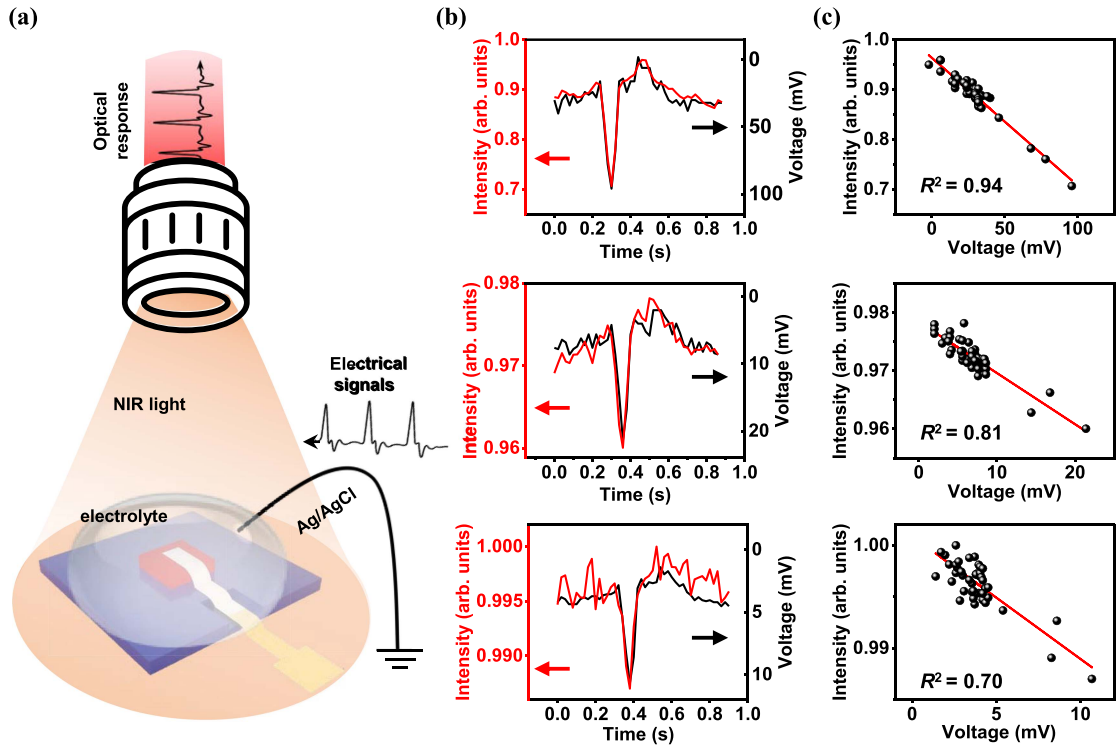

Fig. 4. Optical recording of bioelectrical signals with the heterogeneously integrated sensor. (a) Schematic diagram of the experimental setup, showing synthesized electrocardiogram (ECG) signals applied to the Ag/AgCl electrode in 10 mM NaCl solution, and a camera-equipped fluorescence microscope capturing the luminescence from the device in the electrolyte. (b) Measured luminescence changes (red) in response to the synthesized ECG signals (black) with various peak voltages (top: 100 mV; middle: 20 mV; bottom: 10 mV). (c) Corresponding measured optical signals versus input voltages (black dots), with coefficients of determination obtained by linear fitting (red line).

in the depletion mode, relying on the gate voltage controlled doping of the PEDOT:PSS channel within the ionic electrolyte. Fig. 3(d) plots the measured transfer curve and corresponding transconductance at $V_D = -0.6$ V. Such an OECT obtains its peak transconductance ($\sim$1.5 mS mm^{-1}) at V_G close to 0 V, indicating that it holds the optimal amplification and detection capabilities for weak input voltage signals. The hole mobility extracted from the measured transistor curves is about 1.4 cm^2 V^{-1} s^{-1}. When combining these components (DJPD, LED and OECT) in the circuit configuration shown in Fig. 1(a), different input voltages applied through the gate electrode or different ion concentrations in the electrolyte can alter the channel conductance and thereby adjust the current flowing through the LED, presenting variations of the luminescent intensity. Therefore, the heterogeneously integrated sensor exhibits an electrically and chemically dependent upconversion emission.

To showcase the device's electrical sensing capability, synthesized waveforms are created via a function generator to emulate *in vivo* electrocardiography (ECG) signals. Schematically illustrated in Fig. 4(a), the input voltage signals have varied peak amplitudes of 10–100 mV and a frequency of 1 Hz, feeding into the gate electrode. The luminescence intensity changes emitting from the sensor are recorded by a fluorescence microscope in real-time. The device is immersed in a 10 mM NaCl solution, and an Ag/AgCl wire is used as the gate electrode to deliver the synthesized signals. Fig. 4(b) compares the dynamic optical outputs against the voltage inputs at different amplitudes (100, 20, and 10 mV), suggesting that optical readouts recorded from the integrated sensor are in good accordance with the input electrical signals. Obtained by linear fitting, calculated coefficients of determination are 0.94, 0.81 and 0.70 for input amplitudes of 100, 20, and 10 mV, respectively (Fig. 4(c)). It must be admitted that capturing real ECG signals (with an amplitude typically less than 1 mV) remains challenging for our current sensor, due to the fluctuations of luminescence associated with the excitation source, as well as the limited amplification capability of the OECT. However, the sensing performance can be further improved by optimizing the device geometry and fine tuning the optical setup. Nevertheless, the device prototype exhibits the utility of effectively detecting bioelectrical signals in a wireless manner.

In addition to bioelectrical signals, biochemical cues such as calcium ions (Ca^{2+}) and various neurotransmitters (for example, dopamine) are important biomarkers that highly correlate to biological activities at both cellular and system levels [29]. Since the PEDOT:PSS based OECT also owns a channel conductance sensitive to cation concentrations in the electrolyte, we leverage this feature in the integrated device for selective Ca^{2+} detection. Illustrated in Fig. 5(a), the integrated sensor is immersed in an aqueous solution, and droplets of $CaCl_2$ or NaCl are added to alter the cation concentrations. In particular, a Ca^{2+} selective membrane is coated on the surface of the Ag/AgCl electrode for specific Ca^{2+} detection. Fig. 5(b) plots theoretically calculated current–voltage curves for the DJPD (under excitation

Authorized licensed use limited to: Tsinghua University. Downloaded on November 12,2022 at 07:43:25 UTC from IEEE Xplore. Restrictions apply.

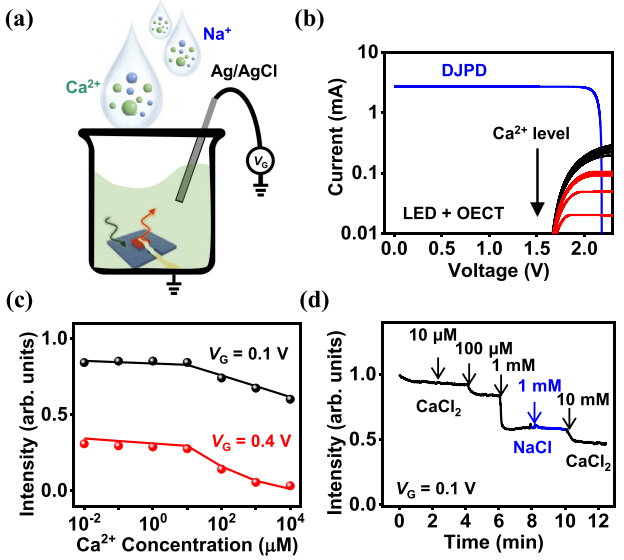

Fig. 5. Optical recording of Ca^{2+} concentration changes in aqueous solutions with the heterogeneously integrated sensor. (a) Schematic illustration of ion concentration measurement by immersing the sensor into the solution. A Ca^{2+} selective membrane is coated on the Ag/AgCl gate electrode. Green dots, Ca^{2+}; Blue dots, Na^{+}. (b) Calculated current–voltage curves of individual devices (DJPD and the series connected LED + OECT) with V_G of 0.1 V (black) and 0.4 V (red), at various levels of $CaCl_2$ from 10 nM to 10 mM (from top to bottom). (c) Calculated (lines) and measured (dots) luminescence intensity as a function of $CaCl_2$ concentration. (d) Dynamic changes of luminescence responding to successive additions of $CaCl_2$ (dark line) compared with the control group of NaCl (blue line).

of 80 mW cm^{-2}) and serially connected LED+OECT in the solution with different Ca^{2+} concentrations, at V_G of 0.1 V (black) and 0.4 V (red). Under both gate voltages, increased Ca^{2+} concertations lead to low channel conductance for OECT and thereby smaller currents injected into the LED. Therefore, the intersection points correspond to the LED luminescence at different Ca^{2+} concentrations, which are plotted in Fig. 5(c), and measured results (dots) are in good agreement with calculations (lines). Fig. 5(d) further shows a continuous measurement of device emission intensity that dynamically changes with added ions. The device luminescence exhibits instantaneous decreases with the increased Ca^{2+} concentration, while the addition of Na^{+} droplets does not alter the optical signal, due to the employment of the Ca^{2+} selective coating.

III. Conclusion

To summarize, we develop an optical based bioelectrical and chemical sensor via heterogeneous integration. Facilitated by transfer printing, a III–V based optoelectronic device and an organic based transistor are combined in the same flexible platform. We theoretically investigate the working mechanism of such a hybrid sensor design, and experimentally demonstrate its ability of optical response to both input voltage and ion concentration changes. Compared with previously reported sensing strategies based on wired electrodes or genetically encoded optical indicators, our device design implies a great potential for realizing non-genetic, optical based monitoring of biological activities at a large scale. Future efforts include the device optimization for improved sensitivity (for example, < 1 mV for ECG recording, < 1 μM for Ca^{2+} detection), miniaturized footprint (size < 10 μm for cellular recording), and large arrays (> 1000 channels) for high-throughput monitoring. These results suggest new possibilities for the integration of optical and electrical semiconductor materials and structures with diverse properties and functions, and provide an advanced tool for biomedical applications.

IV. Methods

A. Theoretical Calculation

Based on the detailed balance theory, the output current from a photodiode I_{PD} is equal to the difference between generated carriers and recombined carriers, and the injected current into an LED converts to photons via the radiative recombination and phonons via the non-radiative recombination.

$$I_{PD} = I_{ph\_PD} + I_{th\_PD} - I_{rad\_PD} - I_{nrad\_PD} \tag{1}$$

$$I_{LED} = -I_{th\_LED} + I_{rad\_LED} + I_{nrad\_LED} \tag{2}$$

I_{ph} is the photogenerated current derived from the excitation light, I_{th} is the absorbed thermal radiation from the environment, I_{rad} is the radiative current, and I_{nrad} is the non-radiative current:

$$I_{th} = \frac{2\pi(n^2+1)qkTS}{h^3c^2} E_g^2 \exp\left(-\frac{E_g}{kT}\right) \tag{3}$$

$$I_{rad} = I_{th} \exp\left(\frac{qV}{kT}\right) \tag{4}$$

$$I_{nrad} = \frac{I_{rad}}{\eta} - I_{rad} \tag{5}$$

where k is Boltzmann's constant, n is the refractive index, S is the surface area of the device, T is Temperature, c is light speed, h is Plank constant, and η is the internal conversion efficiency.

The drain current (I_D) of the PEDOT:PSS-based OECT is determined by the interplay between ionic and electronic motion, in which the effective dopant density distributed in the organic film determines its conductive behavior [23].

$$PEDOT^{+} : PSS^{-} + M^{+} \rightleftarrows PEDOT^{+} + M^{+} : PSS^{-} \tag{6}$$

The effective gate voltage (V_G^{eff}) of the OECT is the sum of the applied gate voltage (V_G) from the external electrical source and the offset voltage (V_{off}) related to the ion concentration. In addition, this offset voltage is derived from the electrolyte potential and is increased with the carrier concentration according to the Nernst equation [26]:

$$\begin{aligned} V_G^{eff} &= V_G + V_{offset} \\ &= V_G + A + \frac{kT}{nq} \ln\left(M^{n+}\right) \end{aligned} \tag{7}$$

Where A is the constant, k is Boltzmann's constant, T is the temperature, n is the number of transferred charges of the cation, q is the elementary charge, M^{n+} is the molar concentration denotes a cation from the electrolyte.

Authorized licensed use limited to: Tsinghua University. Downloaded on November 12,2022 at 07:43:25 UTC from IEEE Xplore. Restrictions apply.

Based on the relation among the drain voltage (V_{D}), the effective gate voltage ($V_{\mathrm{G}}^{\mathrm{eff}}$), and the pinch-off voltage (V_{P}) for this OECT structure from the literature, the drain current I_{D} can be divided into two regions [30]:

$$I_{\mathrm{D}} = \begin{cases} \mu C^* \frac{W \cdot T}{L} \left(V_{\mathrm{P}} - V_{\mathrm{G}}^{\mathrm{eff}} + V_{\mathrm{D}}/2\right) V_{\mathrm{D}} & , V_{\mathrm{D}} \geq V_{\mathrm{G}}^{\mathrm{eff}} - V_{\mathrm{P}} \\ -\mu C^* \frac{W \cdot T}{2L} \left(V_{\mathrm{P}} - V_{\mathrm{G}}^{\mathrm{eff}}\right)^2 & , V_{\mathrm{D}} < V_{\mathrm{G}}^{\mathrm{eff}} - V_{\mathrm{P}} \end{cases} \tag{8}$$

where L, W and T are the length, width and thickness of the channel, μ is the hole mobility, $C^* = c_{\mathrm{d}} / T$ is volume capacitance, V_{D} is the applied source-drain voltage, $V_{\mathrm{P}} = qTp_0/c_{\mathrm{d}}$, and p_0 is the initial hole density in the organic semiconductor before the application of a gate voltage, p is the hole density and c_{d} is the capacitance per unit area.

The heterogeneously integrated sensor comprises a GaAs-based DJPD, an InGaP-based LED, and a PEDOT:PSS OECT. Since these components are connected in series, the current (I) flowing into these three components (I_{PD}, I_{LED}, I_{D}) is matched and is determined by the minimum value. In addition, The output voltage of the DJPD (V_{PD}) is equal to the sum of the voltage of the LED (V_{LED}) and OECT (V_{D}).

$$\begin{cases} V_{\mathrm{PD}} = V_{\mathrm{LED}} + V_{\mathrm{D}} \\ I = \min\left\{I_{\mathrm{PD}}, I_{\mathrm{LED}}, I_{\mathrm{D}}\right\} \end{cases} \tag{9}$$

By solving (9), we can obtain the theoretical curves for emission intensity as a function of the gate voltage in Fig. 2(c).

B. Device Fabrication

The optoelectronic upconversion device with an InGaP-based LED and a GaAs-based DJPD is sequentially grown on the GaAs substrate by metal-organic chemical vapor deposition (MOCVD). The detailed device structure and fabrication process can be found in our previous work [19]. After transfer printing the upconversion device onto a polyimide substrate, a PEDOT:PSS layer is patterned and interconnected with the anodes of LED and photodiode to form an OECT. The PEDOT:PSS (PH-1000, Heraeus Clevios GmbH) is mixed with 5% ethylene glycol as a conductivity enhancer, 1% 3-glycidoxypropyltrimethoxysilane (GOPS) as a crosslinker, 0.25 vol% dodecyl benzene sulfonic acid (DBSA) as a wetting agent. The blended solution is stirred well for 1 hour prior to filtering with the size of a 0.45 μm syringe filter. The filtered solution is spin-coated on the transferred upconversion devices (500 rpm for 10 s, and 2000 rpm for 30 s), and annealed at 130 °C for 20 min. The PEDOT:PSS based layer is patterned by a reactive-ion etching process with O_2 plasma (100 W, 90 mTorr, 100 sccm O_2, 5 sccm SF_6, 120 s), with a lithographically defined photoresist layer for masking (SPR 220-3.0, MicroChemicals). Finally, the integrated device is encapsulated by a SU-8 3005 epoxy layer, with only the channel of the OECT exposed.

The Ca^{2+} selective solution is prepared by dissolving 3.2 mg calcium ionophore II (ETH 129, Sigma-Aldrich Corp.), 1.5 mg sodium tetraphenylborate (NaTPB), 97.9 mg high-molecular-weight polyvinyl chloride (PVC), and 190.3 mg bis(2-ethylehexyl) sebacate (DOS) in 1780 μL tetrahydrofuran. A Ag/AgCl wire is successively dip-coated with the PEDOT:PSS and the Ca^{2+} selective solutions. After drying at room temperature for 24 hours, the Ca^{2+} selective membrane is formed on the PEDOT:PSS-modified Ag/AgCl electrode [29].

C. Device Characterization

Current–voltage curves are recorded using a Keithley 2400 SourceMeter and a 4200A-SCS Parameter Analyzer. The 10 mM sodium chloride (NaCl) aqueous solution is used as the electrolyte in the OECT characterization, which is contained within a customized PDMS well. The Ag/AgCl wire as the gate electrode is immersed in the electrolyte and connected with the source electrode, which is also the anode of the photodiode.

The luminescence photos of the integrated sensor are captured by an Andor Zyla 4.2Plus CMOS camera with an Olympus IX53 microscope equipped with a Xenon arc lamp, which excitation light and the emission light pass through a set of fluorescence filters (EX ET800/60, BS T700spxr-UF1, EM ET650sp, Chroma Tech. Corp.).

ACKNOWLEDGMENT

The authors also acknowledge fabrication and characterization facilities supported by Beijing Institute of Technology Analysis and Testing Center and Tsinghua Nanofabrication Technology Center.

REFERENCES

[1] A. E. Rochford, A. Carnicer-Lombarte, V. F. Curto, G. G. Malliaras, and D. G. Barone, "When bio meets technology: Biohybrid neural interfaces," *Adv. Mater.*, vol. 32, no. 15, 2020, Art. no. 1903182.

[2] R. Liu et al., "High density individually addressable nanowire arrays record intracellular activity from primary rodent and human stem cell derived neurons," *Nano Lett.*, vol. 17, no. 5, pp. 2757–2764, 2017.

[3] M. Dipalo et al., "Plasmonic meta-electrodes allow intracellular recordings at network level on high-density CMOS-multi-electrode arrays," *Nature Nanotechnol.*, vol. 13, no. 10, pp. 965–971, 2018.

[4] S. P. Lacour, G. Courtine, and J. Guck, "Materials and technologies for soft implantable neuroprostheses," *Nature. Rev. Mater.*, vol. 1, no. 10, 2016, Art. no. 16063.

[5] N. Koshiya and J. C. Smith, "Neuronal pacemaker for breathing visualized in vitro," *Nature*, vol. 400, no. 6742, pp. 360–363, 1999.

[6] M. E. Spira and A. Hai, "Multi-electrode array technologies for neuroscience and cardiology," *Nature Nanotechnol.*, vol. 8, no. 2, pp. 83–94, 2013.

[7] P. Fattahi, G. Yang, G. Kim, and M. R. Abidian, "A review of organic and inorganic biomaterials for neural interfaces," *Adv. Mater.*, vol. 26, no. 12, pp. 1846–1885, 2014.

[8] J. J. Jun et al., "Fully integrated silicon probes for high-density recording of neural activity," *Nature*, vol. 551, pp. 232–236, 2017.

[9] A. Barbaglia et al., "Mirroring action potentials: Label-free, accurate, and noninvasive electrophysiological recordings of human-derived cardiomyocytes," *Adv. Mater.*, vol. 33, no. 7, 2021, Art. no. 2004234.

[10] Y. Zhou, E. Liu, H. Müller, and B. Cui, "Optical electrophysiology: Toward the goal of label-free voltage imaging," *J. Amer. Chem. Soc.*, vol. 143, no. 28, pp. 10482–10499, 2021.

[11] R. Elnathan et al., "Biointerface design for vertical nanoprobes," *Nature Rev. Mater.*, vol. 32, pp. 795–803, 2022.

[12] M. S. Siegel and E. Y. Isacoff, "A genetically encoded optical probe of membrane voltage," *Neuron*, vol. 19, no. 4, pp. 735–741, 1997.

[13] H. H. Yang et al., "Subcellular imaging of voltage and calcium signals reveals neural processing in vivo," *Cell*, vol. 166, no. 1, pp. 245–257, 2016.

Authorized licensed use limited to: Tsinghua University. Downloaded on November 12,2022 at 07:43:25 UTC from IEEE Xplore. Restrictions apply.

[14] G. Hong et al., "A method for single-neuron chronic recording from the retina in awake mice," *Science*, vol. 360, no. 6396, pp. 1447–1451, 2018.
[15] Y. Adam et al., "Voltage imaging and optogenetics reveal behaviour-dependent changes in hippocampal dynamics," *Nature*, vol. 569, no. 7756, pp. 413–417, 2019.
[16] A. Habib et al., "Electro-plasmonic nanoantenna: A nonfluorescent optical probe for ultrasensitive label-free detection of electrophysiological signals," *Sci. Adv.*, vol. 5, no. 10, 2019, Art. no. eaav9786.
[17] R. Weissleder, "A clearer vision for in vivo imaging," *Nature Biotechnol.*, vol. 19, no. 4, pp. 316–317, 2001.
[18] F. Zhang, *Photon Upconversion Nanomaterials*. New York, NY, USA: Springer, 2015.
[19] H. Ding et al., "Microscale optoelectronic infrared-to-visible upconversion devices and their use as injectable light sources," *Proc. Nat. Acad. Sci. United States Amer.*, vol. 115, no. 26, pp. 6632–6637, 2018.
[20] H. Ding et al., "An optoelectronic thermometer based on microscale infrared-to-visible conversion devices," *Light Sci. Appl.*, vol. 11, no. 1, 2022, Art. no. 130.
[21] H. Ding et al., "Power- and Spectral-Dependent photon-recycling effects in a double-junction gallium arsenide photodiode," *ACS Photon.*, vol. 6, no. 1, pp. 59–65, 2019.
[22] H. Ding et al., "Optoelectronic sensing of biophysical and biochemical signals based on photon recycling of a micro-LED," *Nano Res.*, vol. 14, no. 9, pp. 3208–3213, 2021.
[23] J. Rivnay et al., "Organic electrochemical transistors," *Nature Rev. Mater.*, vol. 3, no. 2, 2018, Art. no. 17086.
[24] P. Leleux et al., "Organic electrochemical transistors for clinical applications," *Adv. Healthcare Mater.*, vol. 4, no. 1, pp. 142–147, 2015.
[25] D. Khodagholy et al., "In vivo recordings of brain activity using organic transistors," *Nature Commun.*, vol. 4, no. 1, 2013, Art. no. 1575.
[26] P. Lin, F. Yan, and H. L. W. Chan, "Ion-Sensitive properties of organic electrochemical transistors," *ACS Appl. Mater. Interfaces*, vol. 2, no. 6, pp. 1637–1641, 2010.
[27] Y. Deng et al., "A flexible and highly sensitive organic electrochemical transistor-based biosensor for continuous and wireless nitric oxide detection," *Proc. Nat. Acad. Sci.*, vol. 119, no. 34, 2022, Art. no. e2208060119.
[28] S. Park et al., "Self-powered ultra-flexible electronics via nano-grating-patterned organic photovoltaics," *Nature*, vol. 561, no. 7724, pp. 516–521, 2018.
[29] W. Ling et al., "Flexible electronics and materials for synchronized stimulation and monitoring in multi-encephalic regions," *Adv. Funct. Mater.*, vol. 30, no. 32, 2020, Art. no. 2002644.
[30] D. A. Bernards and G. G. Malliaras, "Steady-State and transient behavior of organic electrochemical transistors," *Adv. Funct. Mater.*, vol. 17, no. 17, pp. 3538–3544, 2007.

He Ding received the Ph.D. degree from the Ecole Centrale de Lyon, Écully, France, in 2016, and followed by Postdoctoral Studies with Tsinghua University, Beijing, China, from 2016 to 2018.

He is currently an Assistant Professor with the School of Optics and Photonics, Beijing Institute of Technology, Beijing, China.

Yanxiu Peng received the B.S. degree from the School of Sciences, Nanchang University, Nanchang, China, in 2021.

She is currently working toward the M.S. degree with the School of Optics and Photonics, Beijing Institute of Technology, Beijing, China.

Guoqing Lv received the B.S. degree in 2019 from the School of Optics and Photonics, Beijing Institute of Technology, Beijing, China, where he is currently working toward the M.S. degree.

Yang Xie received the B.Eng. degree from the School of Materials Science and Engineering, Harbin Institute of Technology, Harbin, China, in 2019.

He is currently working toward the Ph.D. degree with the Department of Electronic Engineering, Tsinghua University, Beijing, China.

Junyu Chen received the B.Eng. degree in 2022 from Department of Electronic Engineering, Tsinghua University, Beijing, China, where he is currently working toward the Ph.D. degree.

Zhao Shi received the B.Eng. degree from the School of Optical and Electronic Information, Huazhong University of Science and Technology, Wuhan, China, in 2017.

He is currently working toward the Ph.D. degree with the Department of Electronic Engineering, Tsinghua University, Beijing, China.

Yuping Deng received the B.Eng. degree from the Material Science and Engineering, University of Science and Technology Beijing, Beijing, China, in 2018.

He is currently working toward the Ph.D. degree with the School of Materials Science and Engineering, Tsinghua University, Beijing.

Lan Yin received the bachelor's degree from Tsinghua University, Beijing, China, and the Ph.D. degree from Carnegie Mellon University, Pittsburgh, PA, USA. She is currently an Associate Professor with the School of Materials Science and Engineering, Tsinghua University.

Jian Yang received the Ph.D. degree in optical engineering from the Beijing Institute of Technology, Beijing, China, in 2007.

He is currently a Professor with the School of Optics and Photonics, Beijing Institute of Technology.

Yongtian Wang received the Ph.D. degree in optics from the University of Reading, Reading, U.K., in 1986.

He is currently a Professor with the School of Optics and Photonics, Beijing Institute of Technology, Beijing, China.

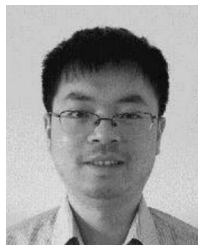

Xing Sheng received the Ph.D. degree from the Massachusetts Institute of Technology, Cambridge, MA, USA, in 2012, and the B.Eng degree from Tsinghua University, Beijing, China, in 2007.

He is currently an Associate Professor with the Department of Electronic Engineering, Tsinghua University.

Authorized licensed use limited to: Tsinghua University. Downloaded on November 12,2022 at 07:43:25 UTC from IEEE Xplore. Restrictions apply.